

Is Signed Message Essential for Graph Neural Networks?

Yoonhyuk Choi¹, Jiho Choi¹, Taewook Ko¹ and Chong-Kwon Kim²

¹Seoul National University

²Korea Institute of Energy Technology

{younhyuk95, jihochoi, taewook.ko}@snu.ac.kr, ckim@kentech.ac.kr

Abstract

Message-passing Graph Neural Networks (GNNs), which collect information from adjacent nodes, achieve satisfying results on homophilic graphs. However, their performances are dismal in heterophilous graphs, and many researchers have proposed a plethora of schemes to solve this problem. Especially, flipping the sign of edges is rooted in a strong theoretical foundation, and attains significant performance enhancements. Nonetheless, previous analyses assume a binary class scenario and they may suffer from confined applicability. This paper extends the prior understandings to multi-class scenarios and points out two drawbacks: (1) the sign of multi-hop neighbors depends on the message propagation paths and may incur inconsistency, (2) it also increases the prediction uncertainty (e.g., conflict evidence) which can impede the stability of the algorithm. Based on the theoretical understanding, we introduce a novel strategy that is applicable to multi-class graphs. The proposed scheme combines confidence calibration to secure robustness while reducing uncertainty. We show the efficacy of our theorem through extensive experiments on six benchmark graph datasets.

1 Introduction

The increase in graph-structured datasets has led to rapid advancements in graph mining techniques including random walk-based node embedding and graph neural networks (GNNs). Especially, GNNs provide satisfactory performances in various applications including node classification and link prediction. The main component of GNNs is message-passing [Gilmer *et al.*, 2017], where the information is propagated between nodes and then aggregated. Also, the integration of a structural property with the node features enhances the representation and the discrimination powers of GNNs substantially [Defferrard *et al.*, 2016; Kipf and Welling, 2016; Velickovic *et al.*, 2017].

Early GNN schemes assume the network homophily where nodes of similar attributes make connections with each other based on the selection [McPherson *et al.*, 2001] or social influence theory [Friedkin, 1998]. Plain GNN algorithms

[Defferrard *et al.*, 2016; Kipf and Welling, 2016] simply perform Laplacian smoothing (a.k.a low-pass filtering) to receive low-frequency signals from neighbor nodes. Consequently, these methods fail to adequately deal with heterophilous graphs [Newman, 2002; Pandit *et al.*, 2007; Zhu *et al.*, 2020] such that even a simple MLP outperforms GNN in some cases. To relieve this problem, a plethora of clever algorithms have been proposed including the adjustment of edge coefficients [Velickovic *et al.*, 2017; Jin *et al.*, 2021; Brody *et al.*, 2021], aggregation of remote nodes with high similarity [Pei *et al.*, 2020; Liu *et al.*, 2021], and diversified message propagation [Yang *et al.*, 2021b]. However, the majority of prior schemes [Ma *et al.*, 2021] stipulate certain conditions of advantageous heterophily and these constraints undermine their generality and applicability.

Recently, some bodies of work allow the edge coefficients to be negative [Chien *et al.*, 2020; Bo *et al.*, 2021] to preserve high-frequency signal exchanges between neighbors. Further, from the perspective of gradient flow, [Bo *et al.*, 2021; Di Giovanni *et al.*, 2022] shows that negative eigenvalue preserves the high-frequency signals to dominate during propagation. [Bodnar *et al.*, 2022] introduces sheaf to enhance the linear separability of neural networks. Instead of changing the signs of edges, others [Luo *et al.*, 2021; Song *et al.*, 2022] assign zero-weights to disassortative connections precluding message diffusion on such edges. Here, there arises a question: *does signed messaging always yield better results than assigning zero-weights on heterophilic edges?*

To answer the above question, we conduct an empirical study and illustrate its results in Figure 1. Along with this, we aim to establish theoretical properties to compare their discrimination power. For this, recent studies [Ma *et al.*, 2021; Yan *et al.*, 2021] scrutinize the changes in node features before and after message reception. Here, they provide some useful insights into using signed messages based on the node’s relative degree and its homophily ratio. Nonetheless, prior analyses were confined to binary class graphs, which may detriment their applicability to generic graphs. In this paper, we extend the theorem to a multi-class scenario positing that the blind application of signed messages to multi-class graphs may increase the uncertainty of predictions. Throughout this analysis, we suggest employing confidence calibration [Guo *et al.*, 2017; Wang *et al.*, 2021] which is simple yet effective to enhance the quality of predictions. To summarize,

our contributions can be described as follows:

- Contrary to prior work confined to a binary class, we tackle the signed messaging mechanism in a multi-class scenario. Our work provides fundamental insight into using signed messages and establishing the theoretical background for the development of powerful GNNs.
- We conjecture and prove that signed messages escalate the inconsistency between neighbors and increase the uncertainty in predictions. Based on this understanding, we propose a novel uncertainty reduction method using confidence calibration.
- We conduct extensive experiments on six benchmark datasets to validate our theorems and show the effectiveness of confidence calibration.

2 Related Work

Graph Neural Networks (GNNs). Under semi-supervised settings, GNNs have shown great potential by utilizing the information of adjacent nodes. Early GNN studies [Bruna *et al.*, 2013; Defferrard *et al.*, 2016] focused on the spectral graph analysis (e.g., Laplacian decomposition) in a Fourier domain. However, they suffer from large computational costs as the scale of the graph increases. GCN [Kipf and Welling, 2016] reduced the overhead by harnessing the localized spectral convolution through the first-order approximation of a Chebyshev polynomial. Another notable approach is spatial-based GNNs [Velickovic *et al.*, 2017; Brody *et al.*, 2021] which aggregate information in a Euclidean domain. Early spatial techniques became a stepping stone to many useful schemes that encompass relevant remote nodes as neighbors.

GNNs on heterophilous graphs. Traditional message-passing GNNs fail to perform well in heterophilic graphs [Pei *et al.*, 2020]. To redeem this problem, recent studies have paid attention to the processing of disassortative edges [Derr *et al.*, 2018; Huang *et al.*, 2019]. They either capture the difference between nodes or incorporate distant but similar nodes as neighbors. For example, H_2 GCN [Zhu *et al.*, 2020] separates ego and neighbors during aggregation. SimP-GCN [Jin *et al.*, 2021] suggests a long-range adjacency matrix and EvenNet [Lei *et al.*, 2022] receives messages from even-hop away nodes only. Similarly, [Li *et al.*, 2022] selects neighbors from the nodes without direct connections. Configuring path-level pattern [Sun *et al.*, 2022] or finding a compatibility matrix [Zhu *et al.*, 2021] has also been proposed. Another school of methodologies either changes the sign of disassortative edges from positive to negative [Chien *et al.*, 2020; Bo *et al.*, 2021; Fang *et al.*, 2022; Guo and Wei, 2022] or assigns zero-weights to disassortative edges [Luo *et al.*, 2021]. Even though these schemes show their effectiveness [Barawal *et al.*, 2021] on binary classes, it may require further investigations before extending their applications to a multi-class scenario.

3 Preliminaries

In this section, let us first define the notations and then explain the basics of the problem.

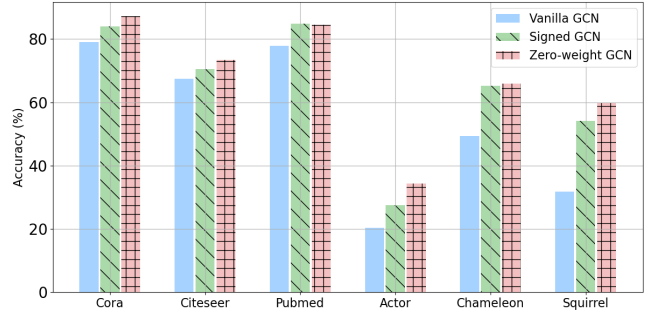


Figure 1: Node classification accuracy on six benchmark datasets. Firstly, vanilla GCN utilizes the original graph. The coefficient of heterophilous edges is changed to -1 in signed GCN and to 0 in zero-weight GCN, respectively

Notations. Let $\mathcal{G} = (\mathcal{V}, \mathcal{E}, X)$ be a graph with $|\mathcal{V}| = n$ nodes and $|\mathcal{E}| = m$ edges. The node attribute matrix is $X \in \mathbb{R}^{n \times F}$, where F is the dimension of an input vector. Given X , the hidden representation of node features $H^{(l)}$ (l -th layer) is derived through message passing. Here, node i 's feature is the row of $h_i^{(l)}$. The structural property of \mathcal{G} can be represented by its adjacency matrix $A \in \{0, 1\}^{n \times n}$. Also, D is a diagonal matrix with node degrees $d_{ii} = \sum_{j=1}^n A_{ij}$. Each node has its label $Y \in \mathbb{R}^{n \times C}$, where C represents the number of classes. The goal of semi-supervised node classification is to predict the class of unlabeled nodes $\mathcal{V}_U = \{\mathcal{V} - \mathcal{V}_L\} \subset \mathcal{V}$ given the partially labeled training set \mathcal{V}_L . The global edge homophily ratio (B) is defined as:

$$B \equiv \frac{\sum_{(i,j) \in \mathcal{E}} \mathbb{1}(Y_i = Y_j)}{|\mathcal{E}|}. \quad (1)$$

Likewise, the local homophily (b_i) of node i is given as:

$$b_i \equiv \frac{\sum_{j=1}^n A_{ij} \cdot \mathbb{1}(Y_i = Y_j)}{d_{ii}}. \quad (2)$$

Empirical Analysis. Vanilla GNNs provide dismal performances in heterophilic datasets, where most edges connect two nodes with different labels. Consequently, finding proper coefficients of entire edges became essential to enhance the overall quality of GNNs. In Fig. 1, we evaluate the node classification accuracy of GCN [Kipf and Welling, 2016] using six benchmark graphs (the statistical details are shown in Table 1). From the original graph (vanilla GCN), we fabricate two graph variants; one that replaces disassortative edges with -1 (signed GCN), and the other that assigns zero-weights on heterophilous connections (zero-weight GCN). As illustrated in Fig. 1, the zero-weight GCN achieves the best performance, followed by the signed GCN. The detailed explanations regarding this phenomenon will be explained in Section 4.2 and 4.3.

4 Theoretical Analysis

We first discuss the mechanism of Message-Passing Neural Networks (MPNN) and the impact of using signed messages (§ 4.1). Then, we introduce the previous analysis of employing signed propagation on binary class graphs (§ 4.2).

Through this, we extend them to a multi-class scenario and point out some drawbacks under this condition (§ 4.3). Finally, we suggest a simple yet effective solution to improve the quality of signed GNNs through the integration of calibration (§ 4.4).

4.1 Message-Passing Neural Networks

Mechanism of Graph Neural Networks (GNNs). Generally, most of the GNNs employ the strategy of propagation and then aggregation, where the node features are updated iteratively. This can be represented as follows:

$$H^{(l+1)} = \phi(\bar{H}^{(l+1)}), \quad \bar{H}^{(l+1)} = AH^{(l)}W^{(l)}. \quad (3)$$

$H^{(0)} = X$ is the initial vector and $H^{(l)}$ is nodes' hidden representations at the l -th layer. $\bar{H}^{(l+1)}$ is retrieved through message-passing (A) and we obtain $H^{(l+1)}$ after an activation function ϕ (e.g. ReLU). $W^{(l)}$ is the trainable weight matrices that are shared across all nodes. The final prediction is produced by applying cross-entropy $\sigma(\cdot)$ (e.g., log-softmax) to $\bar{H}^{(L)}$ and the loss function is defined as:

$$\mathcal{L}_{GNN} = \mathcal{L}_{nll}(Y, \hat{Y}), \quad \hat{Y} = \sigma(\bar{H}^{(L)}). \quad (4)$$

The parameters are updated by computing negative log-likelihood loss \mathcal{L}_{nll} between the predictions (\hat{Y}) and true labels (Y). Most GNN schemes assume that graphs are assortative and they construct the message-passing matrix (A) with positive values to preserve the low-frequency information (local smoothing) [Nt and Maehara, 2019]. Consequently, they fail to capture the difference between node features and achieve lower performance on the heterophilous networks [Oono and Suzuki, 2019; Pei *et al.*, 2020].

Meaning of using signed messages. Recent studies [Chien *et al.*, 2020; Bo *et al.*, 2021; Yan *et al.*, 2021; Chen *et al.*, 2022] emphasize the importance of high-frequency signals and suggest flipping the sign of disassortative edges from positive to negative to preserve such signals. We first show that they can also contribute to the separation of ego and neighbors. Let us assume an ego node i and its neighbor node j is connected with a signed edge. Let us ignore other neighbor nodes to concentrate on the mechanism of signed messaging. Applying GCN [Kipf and Welling, 2016], we obtain the output of node i as:

$$\hat{Y}_i = \sigma(\bar{H}_i^L) = \sigma\left(\frac{\bar{H}_i^{(L)}}{d_i + 1} - \frac{\bar{H}_j^{(L)}}{\sqrt{(d_i + 1)(d_j + 1)}}\right). \quad (5)$$

Assuming that the label of the ego (Y_i) is k , we can calculate the loss (\mathcal{L}_{nll}) between a true label $Y_i \in \mathcal{R}^C$ and a prediction $\hat{Y}_i \in \mathcal{R}^C$ as below:

$$\mathcal{L}_{nll}(Y_i, \hat{Y}_i) = -\log(\hat{y}_{i,k}) \quad (6)$$

Since the column-wise components of the last weight matrix $W^{(L)}$ act as an independent classifier, we prove that the probability of node j being a class k ($\hat{y}_{j,k}$), transitions in the opposite to the node i 's probability ($\hat{y}_{i,k}$) as the training epoch (t) proceeds:

$$\hat{y}_{j,k}^{(t+1)} < \hat{y}_{j,k}^t, \quad \hat{y}_{i,k}^{(t+1)} > \hat{y}_{i,k}^t, \quad (7)$$

where $\hat{y}_{i,k}^{(t+1)} = \hat{y}_{i,k}^t - \eta \nabla_i \mathcal{L}_{nll}(Y_i, \hat{Y}_i)$ and $\hat{y}_{j,k}^{(t+1)} = \hat{y}_{j,k}^t + \eta \nabla_j \mathcal{L}_{nll}(Y_i, \hat{Y}_i)$. Notation η is the learning ratio and a symbol ∇ represents a partial derivative of the loss function. *Proof of Eq. 7 is in App. A.1.*

Motivation. We prove that signed messages contribute to separate disassortative neighbor nodes. Nonetheless, in Fig. 1, signed GCN achieves inferior performance than zero-weighted GCN. In the following section, we analyze this phenomenon by developing our theorems from binary to multi-class scenarios.

4.2 Using signed messages on binary classes

In this section, we aim to analyze the movements of node features given three types of graphs (original, signed, and zero-weights). We again employ GCN [Kipf and Welling, 2016] as a baseline. Here, we assume a binary classification task ($y_i \in \{0, 1\}$) similar to previous work [Baranwal *et al.*, 2021; Yan *et al.*, 2021] and inherit several useful notations for simplifications: (1) For all nodes $i = \{1, \dots, n\}$, their degrees $\{d_i\}$ and features $\{h_i\}$ are i.i.d. random variables. (2) We assume that every class has the same population. (3) With a slight abuse of notation, assume $h^{(0)} = XW^{(0)}$ is the first layer projection of initial node features. (4) Given the label y_i , the node feature follows the distribution (μ or $-\mu$) as:

$$\mathbb{E}(h_i^{(0)}|y_i) = \begin{cases} \mu, & \text{if } y_i = 0 \\ -\mu, & \text{if } y_i = 1. \end{cases} \quad (8)$$

Prior work [Yan *et al.*, 2021] introduces Theorems 4.1, 4.2 using the local homophily (Eq. 2), message passing (Eq. 3), and expectation of node features (Eq. 8). Each theorem below utilizes the original and signed graph, respectively.

Theorem 4.1 (Binary class, vanilla GCN). *Let us assume $y_i = 0$. Then, the expectation after a single-hop propagation $\mathbb{E}(h_i^{(1)})$ is defined as:*

$$\mathbb{E}(h_i^{(1)}|y_i, d_i) = \frac{(2b_i - 1)d'_i + 1}{d_i + 1} \mathbb{E}(h_i^{(0)}|y_i), \quad (9)$$

where $d'_i = \sum_{j \in \mathcal{N}_i} \sqrt{\frac{d_i + 1}{d_j + 1}}$.

Proof is provided in App. A.2.

The generalized version of the above theorem is described in [Ma *et al.*, 2021], which takes two distributions μ_0, μ_1 as:

$$h_i \sim N(b_i\mu_0 + (1 - b_i)\mu_1, \frac{1}{\sqrt{d_i + 1}}). \quad (10)$$

Eq. 10 reduces to Eq. 9 when $\mu_1 = -\mu_0$.

Theorem 4.2 (Binary class, signed GCN). *If the sign of heterophilous edges is flipped correctly under the error ratio (e), the expectation is given by:*

$$\mathbb{E}(h_i^{(1)}|y_i, d_i) = \frac{(1 - 2e)d'_i + 1}{(d_i + 1)} \mathbb{E}(h_i^{(0)}|y_i). \quad (11)$$

Proof can be seen in App. A.3.

Referring to this analysis, we can induce the expectation of zero-weight GCN as below:

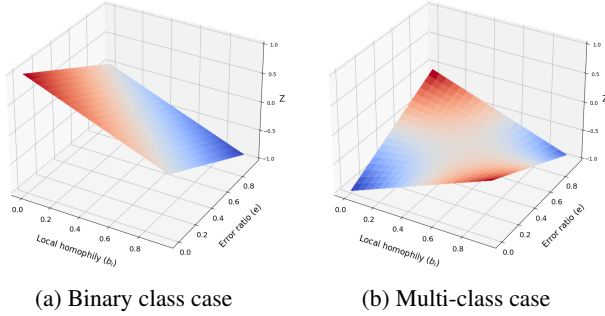


Figure 2: We plot the Z to compare the discrimination power of signed and zero-weight GCNs. The red and blue colored parts indicate the regions where signed GCN and zero-weight GCN have better performance, respectively

Theorem 4.3 (Binary class, zero-weight GCN). *Similar to the Theorem 4.2, assigning zero weights to the heterophilous edges leads to the following feature distribution:*

$$\mathbb{E}(h_i^{(1)}|y_i, d_i) = \frac{(b_i - e)d_i' + 1}{(d_i + 1)} \mathbb{E}(h_i^{(0)}|y_i). \quad (12)$$

Proof can be found in App. A.4.

For all theorems, if the coefficient of $\mathbb{E}(h_i^{(0)}|y_i)$ is smaller than 1, the node feature moves towards the decision boundary and message passing loses its discrimination power [Yan *et al.*, 2021]. Based on this observation, we can compare the discrimination powers of signed and zero-weight GCNs.

Corollary 4.4 (Binary class, discrimination power). *Omitting the overlapping part of Theorems 4.2 and 4.3, their difference, Z , can be induced by the error ratio (e) and homophily (b_i):*

$$Z = (1 - 2e) - (b_i - e) = 1 - e - b_i, \quad (13)$$

where $0 \leq e, b_i \leq 1$.

We visualize Z in Fig. 2a. Note that the space is half-divided by the plane $Z = 0$ since $\int_0^1 \int_0^1 (1 - e - b) de db = 0$. When b_i and e are small, Z becomes positive which indicates that signed GCN outperforms zero-weight GCN and vice versa.

Now, let us assume that the error ratio is zero ($e = 0$) identical to the settings of our previous analysis (Fig. 1). Under this condition, $Z (= 1 - b_i)$ should be non-negative regardless of the homophily ratio ($0 \leq b_i \leq 1$). However, Fig. 1 shows that zero-weight GCN generally outperforms signed GCN ($Z \leq 0$) contradicting the Corollary 4.4. Thus, we extend the above theorems to cover a multi-class scenario and point out the limitations in the previous analyses.

4.3 Using signed messages on multiple classes

Without loss of generality, one can extend the expectation of node features from a binary (Eq. 8) to multiple classes through polar coordinates as below:

$$\mathbb{E}(h_i^{(0)}|y_i) = \left(\mu, \frac{2\pi j}{C}\right), \quad j = 0, \dots, C - 1. \quad (14)$$

Here, μ represents the scale of a vector. The direction of the vector is determined by its label j . The above equation also satisfies the origin symmetry under the binary class ($C = 2$) since $(\mu, 0) = -(\mu, \pi)$. Through this equation, we can redefine Thm. 4.1 and 4.2 for multiple class GCNs.

Theorem 4.5 (Multi-class, signed GCN). *Let us assume the label $y_i = 0$. For simplicity, we denote the coordinates of the ego (μ, θ) as k , and its neighbors (μ, θ') as k' , where $\theta = 0$ and $\theta' = \frac{2\pi j}{C} \neq 0$. Then, the expectation of h_i is defined as:*

$$\mathbb{E}(h_i^{(1)}|y_i, d_i) = \frac{(1 - 2e)\{b_i k + (b_i - 1)k'\}d_i' + k}{d_i + 1}. \quad (15)$$

Proof is provided in App. B.1.

Theorem 4.6 (Multi-class, zero-weight GCN). *Likewise, the $h_i^{(1)}$ driven by zero-weight GCN is:*

$$\mathbb{E}(h_i^{(1)}|y_i, d_i) = \frac{\{(1 - e)b_i k + e(1 - b_i)k'\}d_i' + k}{d_i + 1}. \quad (16)$$

Proof is provided in App. B.2.

Similar to Corollary 4.4, we can compare the separability of the two methods based on their coefficients.

Corollary 4.7 (Multi-class). *The difference of discrimination power (Z) between signed and zero-weight GCN in the multi-class case is:*

$$Z = -eb_i k + (1 - e)(b_i - 1)k' \quad (17)$$

Then, we can induce the conditional statement as below based on the distribution of aggregated neighbors (k'):

$$Z \in \begin{cases} 1 - e - b_i, & \text{if } k' = -k \\ -2eb - (1 - e - b_i), & \text{if } k' = k. \end{cases} \quad (18)$$

More details can be found in App. B.3.

Fig. 2b plots Z for the multi-class case. The above corollary implies that if the distribution of aggregated neighbor is origin symmetry ($k' = -k$), $Z (= 1 - e - b)$ becomes identical to the Eq. 13. Under this condition, signed propagation might perform well. However, as k' gets closer to k , its discrimination power degrades (Z gets smaller) as shown in the blue areas in Fig. 2b, where $\int_0^1 \int_0^1 (-2eb + e + b - 1) dedb = -1$. Intuitively, the probability of being $k' = -k$ may decrease as the number of classes increases, which means that the zero-weight GCN generally outperforms the signed GCN in multi-class graphs. Based on this observation, we point out some limitations below.

Limitation of signed messages in multi-class graphs.

Now, we introduce two types of limitations (P1 and P2) that may degrade the overall quality of GNNs.

(P1) The sign of a message from multi-hop away nodes depend on the paths through which information is transmitted. GNNs stack multiple layers to utilize the information of multi-hop away neighbors. Here, we assume three nodes i, j, k that are connected serially and the signs of their edges are s_{ij} and s_{jk} , respectively. If $y_i = y_j$, then $s_{ij} = 1$, otherwise $s_{ij} = -1$. To begin, let us define a message from node k to i as below:

$$h_i^{(2)} = h_i^{(1)}W^{(1)} + s_{ij}(h_j^{(0)}W^{(0)} + s_{jk}h_k^{(0)}W^{(0)})W^{(1)}, \quad (19)$$

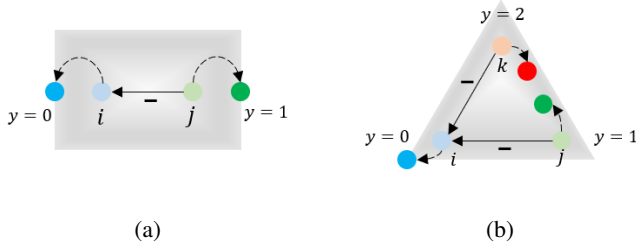


Figure 3: (a) In binary class graphs, signed propagation contributes to the separation of nodes (i, j) and reduces the entropy. (b) In multi-class graphs, the uncertainty of neighboring nodes that are connected with signed edges (j, k) increases

where we omit the degree scaling factor for simplicity. In the above equation, we can infer that the sign of $h_k^{(0)}$ depends on the multiplication of s_{ij} and s_{jk} . If the label is binary (e.g., 0 or 1), signed propagation does not degrade the overall quality since $s_{ij} \cdot s_{jk} = 1$ if i and k belong to the same class, and $s_{ij} \cdot s_{jk} = -1$ otherwise. However, the problem occurs when employing multi-class datasets. For example, let us assume the labels of three nodes are $y_i = 0, y_j = 1$, and $y_k = 2$. Even though i and k are in different classes, k is trained to be similar to i since $s_{ij} \cdot s_{jk} = (-1) \times (-1) = 1$. To solve this problem, one has to configure the classes of nodes on entire paths between two nodes and manually assign their signs. But this incurs high computational costs of $O(\sum_{l=2}^L \sum_{i=1}^N \sum_{j=i}^N A_{ij}^l)$. Thus, we propose to solve the second type of limitation (P2) as below.

(P2) Signed propagation increases the uncertainty of the prediction. Adequate management of uncertainty is vital in machine learning to generate highly confident predictions [DeVries and Taylor, 2018; Moon *et al.*, 2020; Mukherjee and Awadallah, 2020]. This is closely related to the entropy (e.g., information gain [Liu *et al.*, 2022]) and recent work [Kendall and Gal, 2017] formulates two types of uncertainties: the *aleatoric* and *epistemic* caused by the data and the model, respectively. But here, we rather focus on the conflict evidence (*dissonance*) [Perry, 2013; Zhao *et al.*, 2020], which ramps up the entropy of outputs. One can easily measure the uncertainty of a prediction (\hat{y}_i) using Shannon’s entropy [Shannon, 1948] as:

$$E(\hat{y}_i) = - \sum_{j=1}^C \hat{y}_{i,j} \log_c \hat{y}_{i,j}. \quad (20)$$

Furthermore, measuring dissonance (*diss*) is also important [Zhao *et al.*, 2020] as it is powerful in distinguishing Out-of-Distribution (OOD) data from conflict predictions [Huang *et al.*, 2022] and improving classification accuracy:

$$diss(\hat{y}_i) = \sum_{j=1}^C \left(\frac{\hat{y}_{ij} \sum_{k \neq j} \hat{y}_{ik} (1 - \frac{|\hat{y}_{ik} - \hat{y}_{ij}|}{\hat{y}_{ij} + \hat{y}_{ik}})}{\sum_{k \neq j} \hat{y}_{ik}} \right), \quad (21)$$

which can be defined only for non-zero elements. We show that signed messages are helpful for ego and neighbor separation from Eq. 5 to 7. Now, we posit that neighbors con-

Table 1: Statistical details of six benchmark datasets

Datasets	Cora	Citeseer	Pubmed	Actor	Cham.	Squirrel
# Nodes	2,708	3,327	19,717	7,600	2,277	5,201
# Edges	10,558	9,104	88,648	25,944	33,824	211,872
# Features	1,433	3,703	500	931	2,325	2,089
# Labels	7	6	3	5	5	5

nected with signed edges provoke higher entropy (e.g., $E(\hat{y}_i)$ or $diss(\hat{y}_i)$) than the one with a plane or zero-weighted one.

Theorem 4.8. *Under multiple classes, the entropy gap between the signed neighbor $E(\hat{y}_s)$ and plane (or zero) one $E(\hat{y}_p)$ increases in proportion to the training epoch (t) .*

$$E(\hat{y}_s^{(t+1)}) - E(\hat{y}_p^{(t+1)}) > E(\hat{y}_s^t) - E(\hat{y}_p^t). \quad (22)$$

Proof with an example can be seen in the App. C.

To summarize, signed messages contribute to the separation of two nodes (Fig 3a), while they also increase the uncertainty of neighboring nodes j, k that propagate signed information to an ego i (Fig. 3b). To deal with this, we employ confidence calibration which will be explained below.

4.4 Methodology

Previously, we single out two types of limitations. The optimal solution for (P1) is to configure the entire paths between two nodes and assign a proper sign. However, this might be intractable as the size of the graph increases. Instead, we propose a simple yet effective solution that can reduce the uncertainty (P2) through confidence calibration. The proposed method, free from entire path configuration, is cost-efficient and fairly powerful. Calibration is one type of self-training method [Guo *et al.*, 2017; Yang *et al.*, 2021a] that acts as a regularization term. Even though it has shown to be effective for generic GNNs [Wang *et al.*, 2021], we notice that the performance gain is much greater when integrated with signed methods. Many algorithms can be used for calibration (e.g., temperature and vector scaling [Guo *et al.*, 2017]). In this paper, our loss function is defined as,

$$\mathcal{L}_{calib} = \frac{1}{n} \sum_{i=1}^n (-\max(\hat{y}_i) + \text{submax}(\hat{y}_i)), \quad (23)$$

where $n = |\mathcal{V}_{valid} \cup \mathcal{V}_{test}|$ is the set of validation and test nodes. Our method is quite similar to prior work [Wang *et al.*, 2021], but we do not utilize the label of validation sets for a fair comparison. As defined above, it penalizes the maximal and sub-maximal values to be similar in order to suppress the generation of conflict evidence. Since the calibration only utilizes the outputs \hat{y} , it has high scalability and is applicable to any type of GNNs. Integrating Eq. 23, the overall loss (\mathcal{L}_{total}) can be defined as below:

$$\mathcal{L}_{total} = \mathcal{L}_{GNN} + \lambda \mathcal{L}_{calib}. \quad (24)$$

To validate our analysis (§ 5.1), we employ several state-of-the-art methods to obtain \mathcal{L}_{GNN} . The λ is a hyper-parameter that balances the influence of calibration. In Section 5.4, we conduct an experiment to select the λ that achieves the best validation score for each dataset. We describe the pseudo-code and time complexity of our algorithm in App. D.

Table 2: Mean node classification accuracy (%) with standard deviation on six datasets. A shadowed grid indicates the best performance. Values in bracket stand for the dissonance defined in Eq. 21 and symbol ‡ means that calibration is applied to baseline method

Datasets	Cora	Citeseer	Pubmed	Actor	Chameleon	Squirrel
Hom. (Eq. 1)	0.81	0.74	0.8	0.22	0.23	0.22
GCN	79.0 ± 0.6% (0.17)	67.5 ± 0.8% (0.29)	77.6 ± 0.2% (0.53)	20.2 ± 0.4% (0.29)	49.3 ± 0.5% (0.19)	31.7 ± 0.7% (0.31)
GCN‡	81.0 ± 0.9% (0.12)	71.3 ± 1.2% (0.14)	77.8 ± 0.4% (0.38)	21.7 ± 0.6% (0.62)	49.4 ± 0.6% (0.25)	31.5 ± 0.6% (0.58)
APPNP	81.3 ± 0.5% (0.15)	68.9 ± 0.3% (0.21)	79.0 ± 0.3% (0.42)	23.8 ± 0.3% (0.49)	48.0 ± 0.7% (0.34)	30.4 ± 0.6% (0.69)
GAT	80.1 ± 0.6% (0.22)	68.0 ± 0.7% (0.25)	78.0 ± 0.4% (0.45)	22.5 ± 0.3% (0.28)	47.9 ± 0.8% (0.17)	30.8 ± 0.9% (0.27)
GAT‡	81.4 ± 0.4% (0.12)	72.2 ± 0.6% (0.08)	78.3 ± 0.3% (0.39)	23.2 ± 1.8% (0.43)	49.2 ± 0.4% (0.16)	30.3 ± 0.8% (0.40)
GCNII	81.1 ± 0.7% (0.08)	68.5 ± 1.4% (0.13)	78.5 ± 0.4% (0.20)	25.9 ± 1.2% (0.43)	48.1 ± 0.7% (0.21)	29.1 ± 0.9% (0.24)
H ₂ GCN	80.6 ± 0.6% (0.16)	68.2 ± 0.7% (0.22)	78.5 ± 0.3% (0.29)	25.6 ± 1.0% (0.34)	47.3 ± 0.8% (0.19)	31.3 ± 0.7% (0.62)
PTDNet	81.2 ± 0.6% (0.24)	69.5 ± 0.8% (0.42)	78.8 ± 0.5% (0.44)	21.5 ± 0.6% (0.33)	50.8 ± 0.9% (0.17)	32.1 ± 0.7% (0.34)
GPRGNN	82.2 ± 0.4% (0.25)	70.4 ± 0.8% (0.43)	79.1 ± 0.1% (0.26)	25.4 ± 0.2% (0.55)	49.8 ± 0.7% (0.25)	30.5 ± 0.6% (0.36)
GPRGNN‡	84.8 ± 0.2% (0.05)	73.3 ± 0.5% (0.06)	79.9 ± 0.2% (0.14)	27.7 ± 1.3% (0.41)	50.3 ± 0.3% (0.20)	31.0 ± 0.4% (0.17)
FAGCN	80.9 ± 0.5% (0.15)	68.8 ± 0.6% (0.17)	79.0 ± 0.5% (0.31)	25.2 ± 0.8% (0.66)	46.5 ± 1.1% (0.25)	30.4 ± 0.4% (0.64)
FAGCN‡	83.5 ± 0.4% (0.10)	73.4 ± 0.5% (0.08)	79.7 ± 0.2% (0.20)	27.6 ± 0.5% (0.51)	48.6 ± 0.7% (0.20)	31.3 ± 0.5% (0.52)
GGCN	80.0 ± 1.2% (0.38)	68.7 ± 1.6% (0.30)	78.2 ± 0.4% (0.47)	23.0 ± 0.5% (0.47)	48.5 ± 0.7% (0.15)	30.2 ± 0.7% (0.40)
GGCN‡	82.7 ± 0.8% (0.07)	72.2 ± 0.4% (0.05)	78.7 ± 0.3% (0.35)	24.1 ± 0.4% (0.31)	50.3 ± 0.4% (0.08)	30.8 ± 0.6% (0.17)

5 EXPERIMENTS

We conducted extensive experiments to validate our theorems and to compare the performances of our method and baselines. We aim to answer the following research questions:

- **Q1** Is the calibration alleviate the uncertainty issue when integrated with the signed GNNs?
- **Q2** Do the signed messages increase the uncertainty of the final prediction?
- **Q3** Is the number of classes correlated with the prediction uncertainty?
- **Q4** How does the hyper-parameter λ in Eq. 24 affect on the performance?

Datasets. The statistical details of datasets are in Table 1.

(1) *Cora*, *Citeseer*, *Pubmed* [Kipf and Welling, 2016] are citation graphs, where a node corresponds to a paper and edges are citations between them. The labels are the research topic of the papers. (2) *Actor* [Tang *et al.*, 2009] is a co-occurrence graph where actors and co-occurrences in the same movie are represented as nodes and edges, respectively. The labels are five types of actors. (3) *Chameleon*, *Squirrel* [Rozemberczki *et al.*, 2019] are Wikipedia hyperlink networks. Each node is a web page and the edges are hyperlinks. Nodes are categorized into five classes based on monthly traffic.

Baselines. We employ several state-of-the-art methods for validation: (1) Plane GNNs: GCN [Kipf and Welling, 2016], and APPNP [Klicpera *et al.*, 2018]. (2) GNNs for heterophilous graphs: GAT [Velickovic *et al.*, 2017], GCNII [Chen *et al.*, 2020], H₂GCN [Zhu *et al.*, 2020], and PTDNet [Luo *et al.*, 2021]. (3) GNNs with signed propagation: GPRGNN [Chien *et al.*, 2020], FAGCN [Bo *et al.*, 2021], and GGCN [Yan *et al.*, 2021].

Details of implementation and baselines are in App. E.

5.1 Experimental Results (Q1)

In Table 2, we describe the node classification accuracy of each method. A symbol (‡) means that calibration is supplemented to the basic method. Now, let us analyze the results from two perspectives.

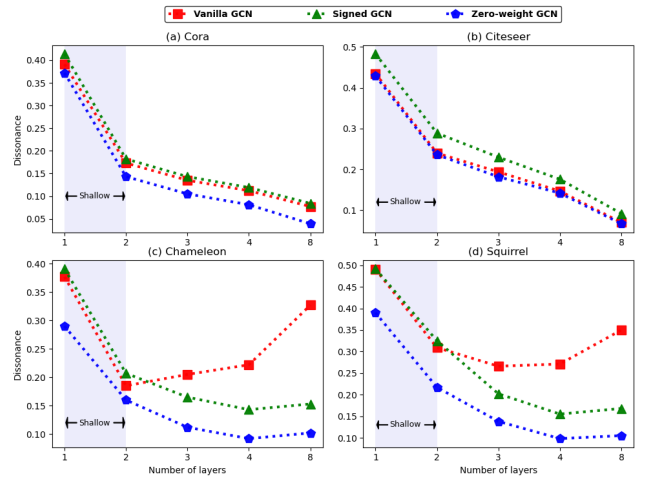


Figure 4: Comparison of the dissonance on three graph variants; vanilla GCN, signed GCN, and zero-weight GCN (Q2)

Homophily ratio plays an important role in GNNs.

Three citation networks have higher homophily compared to others. We can see that all methods perform well under homophilic datasets. As homophily decreases, methods that adjust weights depending on associativity outperform plain GNNs. Similarly, using signed messages (GPRGNN, FAGCN, and GGCN) has shown to be effective here. They achieve notable performance for both homophilic and heterophilic datasets, which means the separation of ego and neighbors (H₂GCN) is quite important.

Calibration improves the overall quality and alleviates uncertainty. We apply calibration (‡) to signed GNNs (GPRGNN, FAGCN, and GGCN). We also apply calibration to GCN and GAT. The average improvements of three signed GNNs by calibration are 4.37%, 3.1%, and 3.13%, respectively. The improvements are greater than those of GCN‡ (2.65%) and GAT‡ (1.97%). Additionally, we describe the dissonance (Eq. 21) of each method in a bracket, where the calibrated methods show lower values than the corresponding

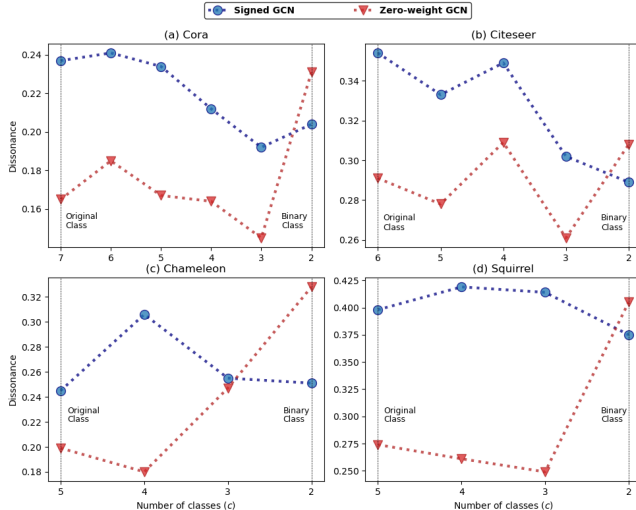


Figure 5: By differentiating the number of classes, we compare the dissonance of GCN using two graph variants (Q3)

vanilla model. To summarize, the results indicate that calibration not only contributes to reducing uncertainty but also improves the accuracy of signed GNNs significantly.

5.2 Correlation of using signed messages and the uncertainty (Q2)

To show that signed messages increase uncertainty, we assume three types of graphs for GCN [Kipf and Welling, 2016] using four datasets. Specifically, we fabricate two graph variants, signed GCN and zero-weight GCN. Here, we remove the randomness for a fair comparison. The results are illustrated in Fig. 4, where the x-axis is the number of layers and the y-axis represents dissonance. Referring to Thm. 4.8, the uncertainty is higher on signed GCN for all shallow layers. As we stack more layers, the entropy of vanilla GCN increases dramatically on heterophilous datasets, the Chameleon and Squirrel. In other words, plain GCN fails to discriminate the ego and neighbors (over-smoothing) and yields low classification accuracy.

5.3 Case Study (Q3)

Theoretical analyses confirm that signed messages increase the uncertainty in multi-class graphs (§ 4.3). They have shown to be effective when k' gets closer to $-k$ (Eq. 18), but this probability is inversely proportional to the number of classes c . To further analyze this phenomenon, we compare the dissonance of two variants of GCN (signed GCN and zero-weight GCN) by decrement of the number of classes (c). Specifically, if the original data contains seven classes (e.g., Cora), we remove all the nodes that belong to the rightmost class to generate a graph with six labels. The results are illustrated in Fig. 5. As can be seen, zero-weight GCN (red) tends to have lower dissonance under multiple classes. However, under binary classes ($c=2$), signed GCN (blue) shows lower uncertainty with the aid of ego-neighbor separation. In the binary case, zero-weight GCN only utilizes homophilous neighbors and fails to generalize under this condition.

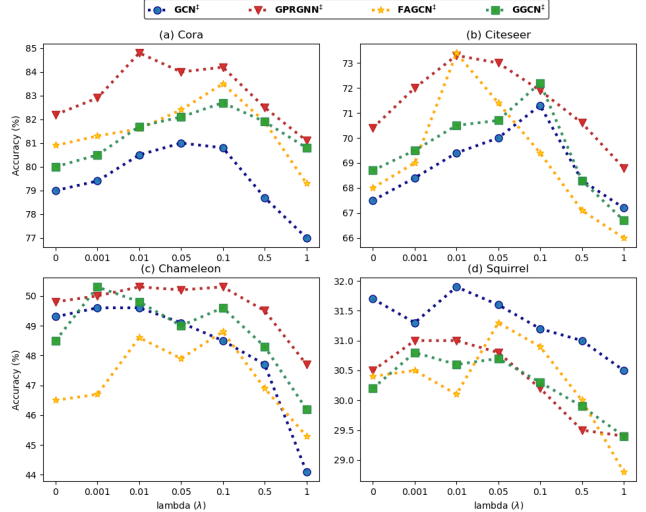


Figure 6: The effect of hyper-parameter λ in Eq. 24 on the classification accuracy of four calibrated methods (Q4)

5.4 Hyper-parameter Analysis (Q4)

We conduct an experiment to investigate the effect of hyper-parameter λ (Eq. 24) that controls the impact of calibration. We tune the λ from 0 to 1 and choose the one with the best validation score. In Figure 6, we describe the node classification accuracy on four benchmark datasets. The blue line represents calibrated GCN, while others are signed GNNs with calibration. Firstly, we notice that GPRGNN^λ achieves the best performance on Cora, Citeseer, and Chameleon datasets. The performance gain in signed GNNs is restricted by the original node classification accuracy. For example, in the Squirrel dataset, GCN outperforms all baselines. Proper calibration helps to improve the performances but is limited by the inherent low capability of base models in heterophilous graphs. Further, assigning the same weights to \mathcal{L}_{GNN} and \mathcal{L}_{calib} generally downgrades the overall performance, which necessitates careful assignment of λ to achieve the optimal results for each dataset.

6 Conclusion

In this work, we provide a new theoretical perspective on using signed messages for node embedding under multi-class benchmark datasets. Firstly, we show that signed messages contribute to the separation of heterophilous neighbors in a binary class, which is consistent with conventional studies. Then, we extend previous theorems to a multi-class scenario and point out two critical limitations of using signed propagation: (1) it may incur inconsistency between nodes, and (2) increases the probability of generating conflict evidence. Based on the observations, we employ calibration for signed GNNs to reduce uncertainty and enhance the quality. Through experimental analysis, we show that our method is beneficial for both homophilic and heterophilic graphs. We claim that our theorems can provide insights to develop a better aggregation scheme for future GNN studies.

References

- [Baranwal *et al.*, 2021] Aseem Baranwal, Kimon Fountoulakis, and Aukosh Jagannath. Graph convolution for semi-supervised classification: Improved linear separability and out-of-distribution generalization. *arXiv preprint arXiv:2102.06966*, 2021.
- [Bo *et al.*, 2021] Deyu Bo, Xiao Wang, Chuan Shi, and Huawei Shen. Beyond low-frequency information in graph convolutional networks. *arXiv preprint arXiv:2101.00797*, 2021.
- [Bodnar *et al.*, 2022] Cristian Bodnar, Francesco Di Giovanni, Benjamin Paul Chamberlain, Pietro Liò, and Michael M Bronstein. Neural sheaf diffusion: A topological perspective on heterophily and oversmoothing in gnns. *arXiv preprint arXiv:2202.04579*, 2022.
- [Brody *et al.*, 2021] Shaked Brody, Uri Alon, and Eran Yahav. How attentive are graph attention networks? *arXiv preprint arXiv:2105.14491*, 2021.
- [Bruna *et al.*, 2013] Joan Bruna, Wojciech Zaremba, Arthur Szlam, and Yann LeCun. Spectral networks and locally connected networks on graphs. *arXiv preprint arXiv:1312.6203*, 2013.
- [Chen *et al.*, 2020] Ming Chen, Zhewei Wei, Zengfeng Huang, Bolin Ding, and Yaliang Li. Simple and deep graph convolutional networks. In *International Conference on Machine Learning*, pages 1725–1735. PMLR, 2020.
- [Chen *et al.*, 2022] Zhixian Chen, Tengfei Ma, and Yang Wang. When does a spectral graph neural network fail in node classification? *arXiv preprint arXiv:2202.07902*, 2022.
- [Chien *et al.*, 2020] Eli Chien, Jianhao Peng, Pan Li, and Olga Milenkovic. Adaptive universal generalized pagerank graph neural network. *arXiv preprint arXiv:2006.07988*, 2020.
- [Defferrard *et al.*, 2016] Michaël Defferrard, Xavier Bresson, and Pierre Vandergheynst. Convolutional neural networks on graphs with fast localized spectral filtering. *Advances in neural information processing systems*, 29, 2016.
- [Derr *et al.*, 2018] Tyler Derr, Yao Ma, and Jiliang Tang. Signed graph convolutional networks. In *2018 IEEE International Conference on Data Mining (ICDM)*, pages 929–934. IEEE, 2018.
- [DeVries and Taylor, 2018] Terrance DeVries and Graham W Taylor. Learning confidence for out-of-distribution detection in neural networks. *arXiv preprint arXiv:1802.04865*, 2018.
- [Di Giovanni *et al.*, 2022] Francesco Di Giovanni, James Rowbottom, Benjamin P Chamberlain, Thomas Markovich, and Michael M Bronstein. Graph neural networks as gradient flows. *arXiv preprint arXiv:2206.10991*, 2022.
- [Fang *et al.*, 2022] Zheng Fang, Lingjun Xu, Guojie Song, Qingqing Long, and Yingxue Zhang. Polarized graph neural networks. In *Proceedings of the ACM Web Conference 2022*, pages 1404–1413, 2022.
- [Friedkin, 1998] Noah E Friedkin. *A structural theory of social influence*. Cambridge University Press, 1998.
- [Gilmer *et al.*, 2017] Justin Gilmer, Samuel S Schoenholz, Patrick F Riley, Oriol Vinyals, and George E Dahl. Neural message passing for quantum chemistry. In *International conference on machine learning*, pages 1263–1272. PMLR, 2017.
- [Guo and Wei, 2022] Yuhe Guo and Zhewei Wei. Clenshaw graph neural networks. *arXiv preprint arXiv:2210.16508*, 2022.
- [Guo *et al.*, 2017] Chuan Guo, Geoff Pleiss, Yu Sun, and Kilian Q Weinberger. On calibration of modern neural networks. In *International conference on machine learning*, pages 1321–1330. PMLR, 2017.
- [Huang *et al.*, 2019] Junjie Huang, Huawei Shen, Liang Hou, and Xueqi Cheng. Signed graph attention networks. In *International Conference on Artificial Neural Networks*, pages 566–577. Springer, 2019.
- [Huang *et al.*, 2022] Tiancheng Huang, Donglin Wang, and Yuan Fang. End-to-end open-set semi-supervised node classification with out-of-distribution detection. In *Proceedings of the Thirty-First International Joint Conference on Artificial Intelligence, IJCAI-22*. IJCAI, 2022.
- [Jin *et al.*, 2021] Wei Jin, Tyler Derr, Yiqi Wang, Yao Ma, Zitao Liu, and Jiliang Tang. Node similarity preserving graph convolutional networks. In *Proceedings of the 14th ACM international conference on web search and data mining*, pages 148–156, 2021.
- [Kendall and Gal, 2017] Alex Kendall and Yarin Gal. What uncertainties do we need in bayesian deep learning for computer vision? *Advances in neural information processing systems*, 30, 2017.
- [Kipf and Welling, 2016] Thomas N Kipf and Max Welling. Semi-supervised classification with graph convolutional networks. *arXiv preprint arXiv:1609.02907*, 2016.
- [Klicpera *et al.*, 2018] Johannes Klicpera, Aleksandar Bojchevski, and Stephan Günnemann. Predict then propagate: Graph neural networks meet personalized pagerank. *arXiv preprint arXiv:1810.05997*, 2018.
- [Lei *et al.*, 2022] Runlin Lei, Zhen Wang, Yaliang Li, Bolin Ding, and Zhewei Wei. Evennet: Ignoring odd-hop neighbors improves robustness of graph neural networks. *arXiv preprint arXiv:2205.13892*, 2022.
- [Li *et al.*, 2022] Xiang Li, Renyu Zhu, Yao Cheng, Caihua Shan, Siqiang Luo, Dongsheng Li, and Weining Qian. Finding global homophily in graph neural networks when meeting heterophily. *arXiv preprint arXiv:2205.07308*, 2022.
- [Liu *et al.*, 2021] Meng Liu, Zhengyang Wang, and Shuiwang Ji. Non-local graph neural networks. *IEEE Transactions on Pattern Analysis and Machine Intelligence*, 2021.

- [Liu *et al.*, 2022] Hongrui Liu, Binbin Hu, Xiao Wang, Chuan Shi, Zhiqiang Zhang, and Jun Zhou. Confidence may cheat: Self-training on graph neural networks under distribution shift. In *Proceedings of the ACM Web Conference 2022*, pages 1248–1258, 2022.
- [Luo *et al.*, 2021] Dongsheng Luo, Wei Cheng, Wenchao Yu, Bo Zong, Jingchao Ni, Haifeng Chen, and Xiang Zhang. Learning to drop: Robust graph neural network via topological denoising. In *Proceedings of the 14th ACM International Conference on Web Search and Data Mining*, pages 779–787, 2021.
- [Ma *et al.*, 2021] Yao Ma, Xiaorui Liu, Neil Shah, and Jiliang Tang. Is homophily a necessity for graph neural networks? *arXiv preprint arXiv:2106.06134*, 2021.
- [McPherson *et al.*, 2001] Miller McPherson, Lynn Smith-Lovin, and James M Cook. Birds of a feather: Homophily in social networks. *Annual review of sociology*, pages 415–444, 2001.
- [Moon *et al.*, 2020] Jooyoung Moon, Jihyo Kim, Younghak Shin, and Sangheum Hwang. Confidence-aware learning for deep neural networks. In *international conference on machine learning*, pages 7034–7044. PMLR, 2020.
- [Mukherjee and Awadallah, 2020] Subhabrata Mukherjee and Ahmed Awadallah. Uncertainty-aware self-training for few-shot text classification. *Advances in Neural Information Processing Systems*, 33:21199–21212, 2020.
- [Newman, 2002] Mark EJ Newman. Assortative mixing in networks. *Physical review letters*, 89(20):208701, 2002.
- [Nt and Maehara, 2019] Hoang Nt and Takanori Maehara. Revisiting graph neural networks: All we have is low-pass filters. *arXiv preprint arXiv:1905.09550*, 2019.
- [Oono and Suzuki, 2019] Kenta Oono and Taiji Suzuki. Graph neural networks exponentially lose expressive power for node classification. *arXiv preprint arXiv:1905.10947*, 2019.
- [Pandit *et al.*, 2007] Shashank Pandit, Duen Horng Chau, Samuel Wang, and Christos Faloutsos. Netprobe: a fast and scalable system for fraud detection in online auction networks. In *Proceedings of the 16th international conference on World Wide Web*, pages 201–210, 2007.
- [Pei *et al.*, 2020] Hongbin Pei, Bingzhe Wei, Kevin Chen-Chuan Chang, Yu Lei, and Bo Yang. Geom-gcn: Geometric graph convolutional networks. *arXiv preprint arXiv:2002.05287*, 2020.
- [Perry, 2013] Chris Perry. Machine learning and conflict prediction: a use case. *Stability: International Journal of Security and Development*, 2(3):56, 2013.
- [Rozemberczki *et al.*, 2019] Benedek Rozemberczki, Ryan Davies, Rik Sarkar, and Charles Sutton. Gemsec: Graph embedding with self clustering. In *Proceedings of the 2019 IEEE/ACM international conference on advances in social networks analysis and mining*, pages 65–72, 2019.
- [Shannon, 1948] Claude Elwood Shannon. A mathematical theory of communication. *The Bell system technical journal*, 27(3):379–423, 1948.
- [Song *et al.*, 2022] Zixing Song, Yifei Zhang, and Irwin King. Towards an optimal asymmetric graph structure for robust semi-supervised node classification. In *Proceedings of the 28th ACM SIGKDD Conference on Knowledge Discovery and Data Mining*, pages 1656–1665, 2022.
- [Sun *et al.*, 2022] Yifei Sun, Haoran Deng, Yang Yang, Chunping Wang, Jiarong Xu, Renhong Huang, Linfeng Cao, Yang Wang, and Lei Chen. Beyond homophily: Structure-aware path aggregation graph neural network. In Lud De Raedt, editor, *Proceedings of the Thirty-First International Joint Conference on Artificial Intelligence, IJCAI-22*, pages 2233–2240. International Joint Conferences on Artificial Intelligence Organization, 7 2022. Main Track.
- [Tang *et al.*, 2009] Jie Tang, Jimeng Sun, Chi Wang, and Zi Yang. Social influence analysis in large-scale networks. In *Proceedings of the 15th ACM SIGKDD international conference on Knowledge discovery and data mining*, pages 807–816, 2009.
- [Velickovic *et al.*, 2017] Petar Velickovic, Guillem Cucurull, Arantxa Casanova, Adriana Romero, Pietro Lio, and Yoshua Bengio. Graph attention networks. *stat*, 1050:20, 2017.
- [Wang *et al.*, 2021] Xiao Wang, Hongrui Liu, Chuan Shi, and Cheng Yang. Be confident! towards trustworthy graph neural networks via confidence calibration. *Advances in Neural Information Processing Systems*, 34:23768–23779, 2021.
- [Yan *et al.*, 2021] Yujun Yan, Milad Hashemi, Kevin Swersky, Yaoqing Yang, and Danai Koutra. Two sides of the same coin: Heterophily and oversmoothing in graph convolutional neural networks. *arXiv preprint arXiv:2102.06462*, 2021.
- [Yang *et al.*, 2021a] Han Yang, Kaili Ma, and James Cheng. Rethinking graph regularization for graph neural networks. In *Proceedings of the AAAI Conference on Artificial Intelligence*, volume 35, pages 4573–4581, 2021.
- [Yang *et al.*, 2021b] Liang Yang, Mengzhe Li, Liyang Liu, Chuan Wang, Xiaochun Cao, Yuanfang Guo, et al. Diverse message passing for attribute with heterophily. *Advances in Neural Information Processing Systems*, 34:4751–4763, 2021.
- [Zhao *et al.*, 2020] Xujiang Zhao, Feng Chen, Shu Hu, and Jin-Hee Cho. Uncertainty aware semi-supervised learning on graph data. *Advances in Neural Information Processing Systems*, 33:12827–12836, 2020.
- [Zhu *et al.*, 2020] Jiong Zhu, Yujun Yan, Lingxiao Zhao, Mark Heimann, Leman Akoglu, and Danai Koutra. Beyond homophily in graph neural networks: Current limitations and effective designs. *Advances in Neural Information Processing Systems*, 33:7793–7804, 2020.
- [Zhu *et al.*, 2021] Jiong Zhu, Ryan A Rossi, Anup Rao, Tung Mai, Nedim Lipka, Nesreen K Ahmed, and Danai Koutra. Graph neural networks with heterophily. In *Proceedings of the AAAI Conference on Artificial Intelligence*, volume 35, pages 11168–11176, 2021.

Technical Appendix

A. Proof of Equation 7 and Theorem 4.1, 4.2, 4.3

A.1. Proof of Equation 7

We first show that signed messages can contribute to separating the ego from its neighbors. Let us assume the label of the ego node i is k . A neighbor node j is connected to i with a signed edge. Since the column-wise components of the weight matrix act as an independent classifier, the probabilities that the two nodes belong to the same class k , $\hat{y}_{i,k}, \hat{y}_{j,k}$, at a training epoch t are derived as,

$$\begin{aligned}\hat{y}_{i,k}^{(t+1)} &= \hat{y}_{i,k}^t - \eta \nabla_i \mathcal{L}_{nll}(Y_i, \hat{Y}_i)_k \\ \hat{y}_{j,k}^{(t+1)} &= \hat{y}_{j,k}^t - \eta \nabla_j \mathcal{L}_{nll}(Y_i, \hat{Y}_i)_k\end{aligned}\quad (25)$$

The loss function is defined as $\mathcal{L}_{nll}(Y_i, \hat{Y}_i)_k = -\log(\hat{y}_{i,k})$, where $\hat{Y}_i = \sigma(\bar{H}_i^L) = \sigma\left(\frac{\bar{H}_i^L}{d_i+1} - \frac{\bar{H}_j^L}{\sqrt{(d_i+1)(d_j+1)}}\right)$. The gradient $\nabla_i \mathcal{L}_{nll}(Y_i, \hat{Y}_i)_k$ is well-known to be,

$$\begin{aligned}\nabla_i \mathcal{L}_{nll}(Y_i, \hat{Y}_i)_k &= \frac{\partial \mathcal{L}_{nll}(Y_i, \hat{Y}_i)_k}{\partial \hat{y}_{i,k}} = \frac{\partial \mathcal{L}_{nll}(Y_i, \hat{Y}_i)_k}{\partial \hat{y}_{i,k}} \cdot \frac{\partial \hat{y}_{i,k}}{\partial h_{i,k}^{(L)}} \\ &= -\frac{1}{\hat{y}_{i,k}} \cdot (\hat{y}_{i,k}(1 - \hat{y}_{i,k})) = \hat{y}_{i,k} - 1 < 0\end{aligned}\quad (26)$$

Similarly, the gradient $\nabla_j \mathcal{L}_{nll}(Y_i, \hat{Y}_i)_k$ is given by:

$$\begin{aligned}\nabla_j \mathcal{L}_{nll}(Y_i, \hat{Y}_i)_k &= \frac{\partial \mathcal{L}_{nll}(Y_i, \hat{Y}_i)_k}{\partial \hat{y}_{i,k}} = \frac{\partial \mathcal{L}_{nll}(Y_i, \hat{Y}_i)_k}{\partial \hat{y}_{i,k}} \cdot \frac{\partial \hat{y}_{i,k}}{\partial h_{j,k}^{(L)}} \\ &= -\frac{1}{\hat{y}_{i,k}} \cdot (\hat{y}_{i,k}(1 - \hat{y}_{i,k})(-1)) = 1 - \hat{y}_{i,k} > 0,\end{aligned}\quad (27)$$

where we can infer that $\hat{y}_{i,k}^{(t+1)} > \hat{y}_{i,k}^t$ and $\hat{y}_{j,k}^{(t+1)} < \hat{y}_{j,k}^t$.

A.2. Proof of Theorem 4.1. [Binary class, vanilla GCN [Yan *et al.*, 2021]]

A detailed proof of Theorem 4.1 and 4.2 is provided in [Yan *et al.*, 2021], where we introduce them briefly here. Assume a binary class $y_i \in \{0, 1\}$. Using the aggregation scheme of GCN [Kipf and Welling, 2016], the hidden representation of node i after message-passing $h_i^{(1)}$ is defined as:

$$h_i^{(1)} = \frac{h_i^{(0)}}{d_i + 1} + \sum_{j \in \mathcal{N}_i} \frac{h_j^{(0)}}{\sqrt{(d_i + 1)(d_j + 1)}}\quad (28)$$

As illustrated in Figure 7a (binary class), we assume $h_i \sim N(\mu, \frac{1}{\sqrt{d_i}})$ if $y_i = 0$ and otherwise $h_i \sim N(-\mu, \frac{1}{\sqrt{d_i}})$. Based on the local homophily ratio b_i , Eq. 28 can be extended as:

$$\begin{aligned}\mathbb{E}(h_i^{(1)} | v_i, d_i) &= \frac{\mu}{d_i + 1} + \sum_{j \in \mathcal{N}_i} \left(\frac{b_i}{\sqrt{(d_i + 1)(d_j + 1)}} \mu - \frac{(1 - b_i)}{\sqrt{(d_i + 1)(d_j + 1)}} \mu \right) \\ &= \left(\frac{1}{d_i + 1} + \sum_{j \in \mathcal{N}_i} \frac{2b_i - 1}{\sqrt{(d_i + 1)(d_j + 1)}} \right) \mu \\ &= \left(\frac{1}{d_i + 1} + \frac{2b_i - 1}{d_i + 1} \sum_{j \in \mathcal{N}_i} \frac{\sqrt{d_i + 1}}{\sqrt{d_j + 1}} \right) \mu \\ &= \left(\frac{1 + (2b_i - 1)d'_i}{d_i + 1} \right) \mu.\end{aligned}\quad (29)$$

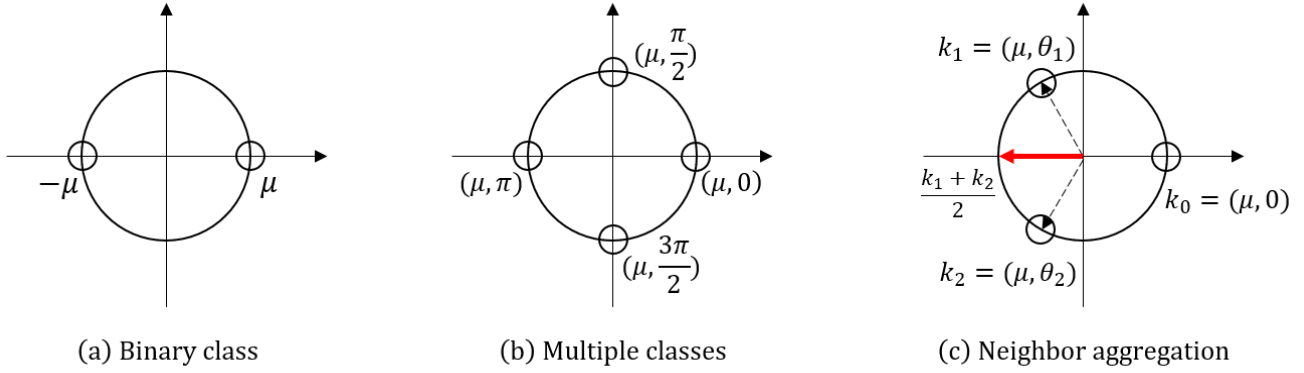


Figure 7: We take an example to illustrate the distribution of node features under (a) binary and (b) multi-class scenarios. Figure (c) represents the aggregation of neighboring nodes (k_1, k_2) under multiple classes

A.3. Proof of Theorem 4.2. [Binary class, signed GCN [Yan *et al.*, 2021]]

Similarly, signed GCN correctly configures the sign of heterophilous edges with the following error ratio $1 - e$. For example, the sign of heterophilous nodes changes from $-\mu$ to μ with a probability $1 - e$ and vice versa:

$$\begin{aligned}
 \mathbb{E}(h_i^{(1)} | v_i, d_i) &= \frac{\mu}{d_i + 1} + \sum_{j \in \mathcal{N}_i} \left(\frac{\mu(1-e) - \mu e}{\sqrt{(d_i+1)(d_j+1)}} b_i + \frac{\mu(1-e) - \mu e}{\sqrt{(d_i+1)(d_j+1)}} (1-b_i) \right) \\
 &= \frac{\mu}{d_i + 1} + \sum_{j \in \mathcal{N}_i} \left(\frac{1-2e}{\sqrt{(d_i+1)(d_j+1)}} \mu \right) \\
 &= \left(\frac{1}{d_i + 1} + \frac{1-2e}{d_i + 1} \sum_{j \in \mathcal{N}_i} \frac{\sqrt{d_i+1}}{\sqrt{d_j+1}} \right) \mu \\
 &= \left(\frac{1 + (1-2e)d'_i}{d_i + 1} \right) \mu.
 \end{aligned} \tag{30}$$

A.4. Proof of Theorem 4.3. [Binary class, zero-weight GCN]

Likewise, we can induce the expectation of zero-weight GCN by assigning zero weights on heterophilous nodes as follows:

$$\begin{aligned}
 \mathbb{E}(h_i^{(1)} | v_i, d_i) &= \frac{\mu}{d_i + 1} + \sum_{j \in \mathcal{N}_i} \left(\frac{\mu(1-e) - \mu e \times 0}{\sqrt{(d_i+1)(d_j+1)}} b_i + \frac{\mu(1-e) \times 0 - \mu e}{\sqrt{(d_i+1)(d_j+1)}} (1-b_i) \right) \\
 &= \frac{\mu}{d_i + 1} + \sum_{j \in \mathcal{N}_i} \left(\frac{b_i - e}{\sqrt{(d_i+1)(d_j+1)}} \mu \right) \\
 &= \left(\frac{1}{d_i + 1} + \frac{b_i - e}{d_i + 1} \sum_{j \in \mathcal{N}_i} \frac{\sqrt{d_i+1}}{\sqrt{d_j+1}} \right) \mu \\
 &= \left(\frac{1 + (b_i - e)d'_i}{d_i + 1} \right) \mu.
 \end{aligned} \tag{31}$$

B. Proof of Theorem 4.5, 4.6, and Corollary 4.7

B.1. Proof of Theorem 4.5. [Multi-class, signed GCN]

As shown in Figure 7b, we extend a binary classification scenario to a multi-class case. Without loss of generality, we employ polar coordinates and ensure that μ corresponds to the scale of a vector, while the direction of each vector lies between zero and $\frac{2\pi}{C}$ with respect to their label j . Here, we assume the label is $y_i = 0$. For simplicity, we replace $(\mu, \theta = 0)$ as k and $(\mu, \theta' \neq \theta)$ as k' , respectively. Though k' comprises multiple distributions that are proportional to the number of classes, their aggregation

always satisfies $|k'_{agg}| \leq \mu$ since the summation of coefficients $(1 - b_i)$ is lower than 1 and $|k'| \leq \mu$. Referring to Fig. 7c, we can see that $\frac{k_1 + k_2}{2} \leq \mu$ given $b_1 = b_2 = 0.5$, where the aggregation of neighbors always lies in μ . Thus, for brevity, we indicate k'_{agg} as k' here. Now, we can retrieve the expectation (h_i) of signed GCN as follows:

$$\begin{aligned}
\mathbb{E}(h_i^{(1)} | v_i, d_i) &= \frac{k}{d_i + 1} + \sum_{j \in \mathcal{N}_i} \left(\frac{k(1-e) - ke}{\sqrt{(d_i+1)(d_j+1)}} b_i + \frac{-k'(1-e) + k'e}{\sqrt{(d_i+1)(d_j+1)}} (1-b_i) \right) \\
&= \frac{k}{d_i + 1} + \sum_{j \in \mathcal{N}_i} \left(\frac{k(1-2e)b_i - k'(1-2e)(1-b_i)}{\sqrt{(d_i+1)(d_j+1)}} \right) \\
&= \frac{k}{d_i + 1} + \sum_{j \in \mathcal{N}_i} \left(\frac{(1-2e)\{kb_i + k'(b_i-1)\}}{\sqrt{(d_i+1)(d_j+1)}} \right) \\
&= \frac{k}{d_i + 1} + \frac{(1-2e)\{kb_i + k'(b_i-1)\}d'_i}{d_i + 1} \\
&= \frac{(1-2e)\{b_i k + (b_i-1)k'\}d'_i + k}{d_i + 1}.
\end{aligned} \tag{32}$$

B.2. Proof of Theorem 4.6. [Multi-class, zero-weight GCN]

Similar to Eq. 32, the expectation of assigning zero weights for multi-class GCN is given by:

$$\begin{aligned}
\mathbb{E}(h_i^{(1)} | v_i, d_i) &= \frac{k}{d_i + 1} + \sum_{j \in \mathcal{N}_i} \left(\frac{k(1-e) - ke \times 0}{\sqrt{(d_i+1)(d_j+1)}} b_i + \frac{k'(1-e) \times 0 + k'e}{\sqrt{(d_i+1)(d_j+1)}} (1-b_i) \right) \\
&= \frac{k}{d_i + 1} + \sum_{j \in \mathcal{N}_i} \left(\frac{k(1-e)b_i + k'e(1-b_i)}{\sqrt{(d_i+1)(d_j+1)}} \right) \\
&= \frac{k}{d_i + 1} + \frac{\{(1-e)b_i k + e(1-b_i)k'\}d'_i}{d_i + 1} \\
&= \frac{\{(1-e)b_i k + e(1-b_i)k'\}d'_i + k}{d_i + 1}.
\end{aligned} \tag{33}$$

B.3. Analysis on Corollary 4.7

Taking Eq. 32 and 33, one can compare the discrimination power between a sign-flip and zero-weight GCN under a multi-class scenario. Exclude the overlapping part $\frac{k}{d_i+1}$, Z can be retrieved as below:

$$\begin{aligned}
Z &= (1-2e)\{b_i k + (b_i-1)k'\} - \{(1-e)b_i k + e(1-b_i)k'\} \\
&= -eb_i k + (1-e)(b_i-1)k'
\end{aligned} \tag{34}$$

As mentioned above, $k' = (\mu', \theta')$ where $0 \leq \mu' \leq \mu$ and $0 \leq \theta' \leq 2\pi$. If the scale of the aggregated vector is $|\mu'| = 0$, $Z = -eb_i k \leq 0$ and this implies zero-weight GCN generally outperforms signed GCN. Instead, assuming the scale as $\mu' = \mu$, Z is determined w.r.t. the angle of k' as follows:

$$Z \in \begin{cases} 1 - e - b, & \text{if } k' = -k \\ -2eb - (1 - e - b), & \text{if } k' = k, \end{cases} \tag{35}$$

Firstly, if k' is origin symmetric to k , the plane Z is half-divided as,

$$\int_0^1 \int_0^1 (1 - e - b) dedb = \left[1 - \frac{e^2 + b^2}{2} \right]_{e,b=0}^1 = 0 \tag{36}$$

However, as k' gets closer to k , we notice that Z tends to be negative as below:

$$\int_0^1 \int_0^1 (-2eb + e + b - 1) dedb = \left[\frac{-eb^2 - e^2b + e^2 + b^2}{2} - 1 \right]_{e,b=0}^1 = -1. \tag{37}$$

Intuitively, the probability of being $k' = -k$ is inversely proportional to the number of entire classes. Thus, one can infer that zero-weight GCN generally outperforms signed one given multi-class datasets.

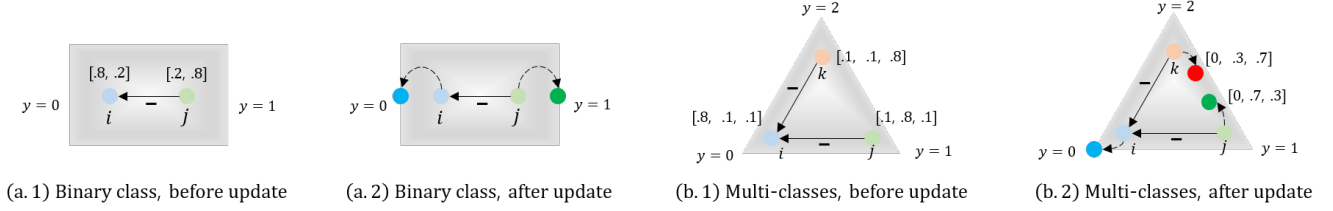


Figure 8: We visualize the update procedure of node features under binary (a.1, a.2) and multi-class scenarios (b.1, b.2)

C. Proof of Theorem 4.8

In § A.1., we proved that signed messages contribute to the separation of ego and neighbors as below:

$$\begin{aligned}\hat{y}_{i,k}^{(t+1)} &= \hat{y}_{i,k}^t - \eta \nabla_i \mathcal{L}_{nll}(Y_i, \hat{Y}_i)_k > \hat{y}_{i,k}^t \\ \hat{y}_{j,k}^{(t+1)} &= \hat{y}_{j,k}^t - \eta \nabla_j \mathcal{L}_{nll}(Y_i, \hat{Y}_i)_k < \hat{y}_{j,k}^t,\end{aligned}\quad (38)$$

in case the label of ego (i) is k , and the neighboring node (j) is connected with a signed edge.

Here, let us assume two nodes s and p , which are connected to a central node i with a signed (s) and plane edge (p), respectively. We aim to show that a difference between the $E(\hat{y}_s)$ and $E(\hat{y}_p)$ increases w.r.t. the training epoch (t) under a multi-class scenario:

$$E(\hat{y}_s^{(t+1)}) - E(\hat{y}_p^{(t+1)}) > E(\hat{y}_s^t) - E(\hat{y}_p^t). \quad (39)$$

Firstly, the true label probability (k) of node p $\hat{y}_{p,k}$ increases, while other probabilities $\hat{y}_{p,o}$ ($o \neq k$) decrease as follows:

$$\hat{y}_p^{(t+1)} \in \begin{cases} \hat{y}_{p,k}^t - \eta \nabla_p \mathcal{L}_{nll}(Y_i, \hat{Y}_i)_k > \hat{y}_{p,k}^t, \\ \hat{y}_{p,o}^t - \eta \nabla_p \mathcal{L}_{nll}(Y_i, \hat{Y}_i)_o < \hat{y}_{p,o}^t, \quad \forall o \neq k. \end{cases} \quad (40)$$

Since we proved that $\nabla_p \mathcal{L}_{nll}(Y_i, \hat{Y}_i)_k < 0$ in Eq. 26, we analyze the partial derivative $\nabla_p \mathcal{L}_{nll}(Y_i, \hat{Y}_i)_o$ ($\forall o \neq k$):

$$\begin{aligned}\nabla_p \mathcal{L}_{nll}(Y_i, \hat{Y}_i)_o &= \frac{\partial \mathcal{L}_{nll}(Y_i, \hat{Y}_i)_o}{\partial \hat{y}_{p,o}} = \frac{\partial \mathcal{L}_{nll}(Y_i, \hat{Y}_i)_o}{\partial \hat{y}_{i,o}} \cdot \frac{\partial \hat{y}_{i,o}}{\partial \hat{h}_{p,o}^{(L)}} \\ &= \frac{1}{\hat{y}_{i,o}} \cdot (\hat{y}_{i,o}(1 - \hat{y}_{i,o})) = 1 - \hat{y}_{i,o} > 0,\end{aligned}\quad (41)$$

which satisfies $\hat{y}_{p,o}^t - \eta \nabla_p \mathcal{L}_{nll}(Y_i, \hat{Y}_i)_o < \hat{y}_{p,o}^t$.

On the contrary, the gradient of node s has a different sign with node p , where we can infer that:

$$\hat{y}_s^{(t+1)} \in \begin{cases} \hat{y}_{s,k}^t - \eta \nabla_s \mathcal{L}_{nll}(Y_i, \hat{Y}_i)_k < \hat{y}_{s,k}^t, \\ \hat{y}_{s,o}^t - \eta \nabla_s \mathcal{L}_{nll}(Y_i, \hat{Y}_i)_o > \hat{y}_{s,o}^t, \quad \forall o \neq k. \end{cases} \quad (42)$$

As the training epoch increases, $\hat{y}_{p,k}$ will converge to 1 resulting in the decrease of $E(\hat{y}_p)$. Conversely, $\hat{y}_{s,k}$ gets closer to 0, which may fail to generate a highly confident prediction and leads to a surge of uncertainty. Thus, one can infer that $E(\hat{y}_s^{(t+1)}) - E(\hat{y}_p^{(t+1)}) > E(\hat{y}_s^t) - E(\hat{y}_p^t)$ as $t \rightarrow \infty$. As shown in Figure 8a, this can be effective under a binary class, while the signed nodes (i, j) in a multi-class case (Fig. 8b) have conflict evidence except for class 0. Taking another example, let us assume that the original probability (before the update) is $\hat{y}_i^t = [0.6, 0.2, 0.2]$ with $C = 3$. Then, one can calculate the Shannon's entropy (E) of \hat{y}_i^t as,

$$E(\hat{y}_i^t) = - \sum_{j=1}^3 \hat{y}_{i,j}^t \log_3 \hat{y}_{i,j}^t \approx 0.8649 \quad (43)$$

Without considering node degree, let us assume the gradient of class k as $\nabla_p \mathcal{L}_{nll}(Y_i, \hat{Y}_i)_k = -\nabla_s \mathcal{L}_{nll}(Y_i, \hat{Y}_i)_k = \alpha$, and other classes as $\nabla_p \mathcal{L}_{nll}(Y_i, \hat{Y}_i)_o = -\nabla_s \mathcal{L}_{nll}(Y_i, \hat{Y}_i)_o = \frac{\alpha}{C-1}$ ($\forall o \neq k$). If we take $\alpha = 0.1$, $\hat{y}_p^{(t+1)}$ and $\hat{y}_s^{(t+1)}$ becomes:

$$E(\hat{y}_p^{(t+1)}) = E([0.8, 0.1, 0.1]) \approx 0.5817, \quad E(\hat{y}_s^{(t+1)}) = E([0.4, 0.3, 0.3]) \approx 0.9911, \quad (44)$$

where we can see that $E(\hat{y}_p^{(t+1)}) < E(\hat{y}_s^{(t+1)})$ after the single iteration.

D. Pseudo-code and Time Complexity of Our Algorithm

D.1. The pseudo-code is as below. For GNNs (line 3), any type of message-passing scheme can be used.

Algorithm 1 Pseudo-code of calibrated GNN

Require: Adjacency matrix (A), node features (X), initialized parameters of GNN (θ), Best validation score ($\alpha^* = 0$)

Ensure: Parameters with the best validation score (θ^*)

- 1: **for** training epochs **do**
 - 2: Retrieve output of GNNs, $\hat{Y} = \sigma(\bar{H}^{(L)})$
 - 3: Compute negative-log likelihood loss, $\mathcal{L}_{GNN} = \mathcal{L}_{nll}(Y, \hat{Y})$
 - 4: Compute calibration loss, $\mathcal{L}_{calib} = \frac{1}{n} \sum_{i=1}^n (-\max(\hat{y}_i) + \text{submax}(\hat{y}_i))$, $n = |\mathcal{V}_{valid} \cup \mathcal{V}_{test}|$
 - 5: Retrieve total loss, $\mathcal{L}_{total} = \mathcal{L}_{GNN} + \lambda \mathcal{L}_{calib}$
 - 6: Update parameters, $\theta' = \theta - \eta \frac{\partial \mathcal{L}_{total}}{\partial \theta}$
 - 7: Through θ' , compute the validation score α
 - 8: **if** $\alpha > \alpha^*$ **then**
 - 9: Save updated parameters, $\theta^* = \theta'$
 - 10: Update best validation score, $\alpha^* = \alpha$
-

D.2. Time complexity of calibrated GNN

We analyze the computational complexity of Algorithm 1. For brevity, we take vanilla GCN [Kipf and Welling, 2016] as a base model. Generally, the cost of GCN is known to be proportional to the number of edges and trainable parameters $\mathcal{O}(|\mathcal{E}| \theta_{GCN})$. Here, θ_{GCN} is comprised of $\mathcal{O}(nz(X)F' + F'C)$ [Zhu *et al.*, 2020], where $nz(\cdot)$ represents the non-zero elements of inputs and F' stand for the hidden dimension, and C is the number of classes. Additionally, the calibration takes $n = |\mathcal{V}_{valid} \cup \mathcal{V}_{test}|$ samples as inputs and finds top k samples on each row of \hat{Y} . Thus, their complexity can be simply defined as $\mathcal{O}(n + k)$. To summarize, the cost of calibrated GCN is $\mathcal{O}(|\mathcal{E}| \theta_{GCN} + n + k)$, which is fairly efficient compared to plane GNNs.

E. More Details about Implementations and Baselines

E.1. General information of the implementations.

All methods including baselines and ours are implemented upon *PyTorch Geometric*¹. For a fair comparison, we equalize the hidden dimension of the entire methodologies as 64. ReLU with dropout is used for non-linearity and to prevent over-fitting. We employ the log-Softmax as a cross-entropy function. The learning ratio is set to $1e^{-3}$ and the Adam optimizer is taken with weight decay $5e^{-4}$. For training, 20 nodes per class are randomly chosen and the remaining nodes are equally divided into two parts for validation and testing.

E.2. More details about baseline methods.

- **GCN** [Kipf and Welling, 2016] is a first-order approximation of Chebyshev polynomials [Defferrard *et al.*, 2016]. For all datasets, we simply take 2 layers of GCN.
- **APPNP** [Klicpera *et al.*, 2018] combines personalized PageRank on GCN. We stack 10 layers and set the teleport probability (α) as $\{0.1, 0.1, 0.1, 0.5, 0.2, 0.3\}$ for Cora, Citeseer, Pubmed, Actor, Chameleon, and Squirrel.
- **GAT** [Velickovic *et al.*, 2017] calculates feature-based attention for edge coefficients. Similar to GCN, we construct 2 layers of GAT. The pair of (hidden dimension, head) is set as (8, 8) for the first layer, while the second layer is (1, number of classes).
- **GCNII** [Chen *et al.*, 2020] integrates an identity mapping function on APPNP. We set $\alpha = 0.5$ and employ nine hidden layers. We increase the weight of identity mapping (β) that is inversely proportional to the heterophily of the dataset.
- **H₂GCN** [Zhu *et al.*, 2020] suggests the separation of ego and neighbors during aggregation. We refer to the publicly available *source code*² for implementation.

¹<https://pytorch-geometric.readthedocs.io/en/latest/modules/nn.html>

²<https://github.com/GemsLab/H2GCN>

- **PTDNet** [Luo *et al.*, 2021] removes disassortative edges before a message-passing. We also utilize the open *source code*³ here.
- **GPRGNN** [Chien *et al.*, 2020] generalized the personalized PageRank to deal with heterophily and over-smoothing. Referring *here*⁴, we tune the hyper-parameters based on the best validation score for each dataset.
- **FAGCN** [Bo *et al.*, 2021] determines the sign of edges using the node features. We implement the algorithm referring *here*⁵ and also tune the hyper-parameters with respect to their accuracy.
- **GGCN** [Yan *et al.*, 2021] proposes the scaling of degrees and the separation of positive/negative adjacency matrices. We simply take the publicly available *code*⁶ for evaluation.

³<https://github.com/flyingdoog/PTDNet>

⁴<https://github.com/jianhao2016/GPRGNN>

⁵<https://github.com/bdy9527/FAGCN>

⁶https://github.com/Yujun-Yan/Heterophily_and_oversmoothing